Supporting Information

Tuning surface segregation composition of PdCo alloy by the atmosphere for increasing electrocatalytic activity

Tongtong Li,‡[a] Rong Wang,‡[b] Minghe Yang,[a] Shuaishuai Zhao,[a] Zhijie Li,[a] Junjian Miao,[b] Zhida Gao,[a] Yi Gao*[bc] and Yanyan Song*[a]

[a] *College of Sciences, Northeastern University, Shenyang 110004, China.*
[b] *Shanghai Institute of Applied Physics, Chinese Academy of Sciences, Shanghai 201800, China.*
[c] *Shanghai Advanced Research Institute, Chinese Academy of Sciences, Shanghai 201800, China.*
**Correspondence to: yysong@mail.neu.edu.cn; gaoyi@sinap.ac.cn*
‡*These authors contributed equally to this work.*

Experimental Section

HER mechanism in acidic solutions

Electrochemical hydrogen adsorption – Volmer reaction:

$$H_3O^+ + e^- \longrightarrow H_{ads} + H_2O$$

Electrochemical desorption – Heyrovsky reaction:

$$H_{ads} + H_3O^+ + e^- \longrightarrow H_2 + H_2O$$

Chemical desorption – Tafel reaction:

$$H_{ads} + H_{ads} \longrightarrow H_2$$

If the Volmer, Heyrovsky or Tafel step is the rate-determining step, the corresponding Tafel slope of ~120, 40 or 30 mV dec^{-1} will be achieved.[1]

TOF calculation

ECSA is used to quantitatively evaluate surface area of metal exposure. The ECSA of the catalyst was determined according to the following equation:

$$\mathrm{ECSA} = \frac{Q}{q}$$

$$= \frac{\int \frac{I \times \delta E}{v}}{q}$$

where ν is the scan rate (50 mV/s). For Pd, q (424 μC cm^{-2})[2] is the charge required for monolayer desorption of oxygen on the Pd surface, and Q is the surface charge obtained from the area under the CV for oxygen desorption (peak located at around 0.65 V *vs.* RHE). For Pt, q (210 μC cm^{-2})[3] is the charge required for monolayer desorption or absorption of hydrogen on the Pt surface, Q is the surface charge obtained from hydrogen absorption and desorption areas in CV curve (0.05 ~ 0.4 V *vs.* RHE).

To calculate the TOF, we used the following formula:

$$\mathrm{TOF} = \frac{\#\, total\ \ hydrogen\ \ turn\, overs\ /\ \ cm^2_{geometric}}{\#\, total\, surface\ sites\ /\, cm^2_{geometric}}$$

The total number of hydrogen turn over is calculated from the current density using the following conversion:

$$\left(\mathrm{j}\ \frac{mA}{cm^2_{geometric}}\right)\left(\frac{1\,A}{1000\,mA}\right)\left(\frac{1\,C/s}{1\,A}\right)\left(\frac{1\,mol\,e^-}{96485.3\,C}\right)\left(\frac{1\,mol\,H_2}{2\,mol\,e^-}\right)\left(\frac{6.02214 * 10^{23}\ molecules\ H_2}{1\,mol\,H_2}\right)$$

$$= 3.12 \times 10^{15}\ \frac{H_2/s}{cm^2_{geometric}}\ per\,\frac{mA}{cm^2_{geometric}}$$

while the number of total surface sites can be obtained from formula:

$$\#\ \mathrm{surface\ sites}\ per\ \mathrm{real\ surface\ area} \times \mathrm{ECSA_{metal}}$$

$$= \left(\frac{6.02214 \times 10^{23}}{1\,mol} \times \frac{1\,mol}{106.42\,g} \times \frac{12.023\,g}{1\,cm^3}\right)^{2/3} \times \mathrm{ECSA_{Pd}}$$

We also use mass loading to calculate the active surface site density and per-site TOF.

$$\mathrm{TOF} = \frac{j \times \ \ 3.12 \times 10^{15}\ \dfrac{H_2/s}{cm^2_{geometric}}\ per \dfrac{mA}{cm^2_{geometric}}}{64.36\% \times \dfrac{0.125\ mg}{cm^2_{geometric}} \times \dfrac{1\ mol}{106.42\ g} \times \dfrac{6.02214 \times 10^{23}}{1\ mol}}$$

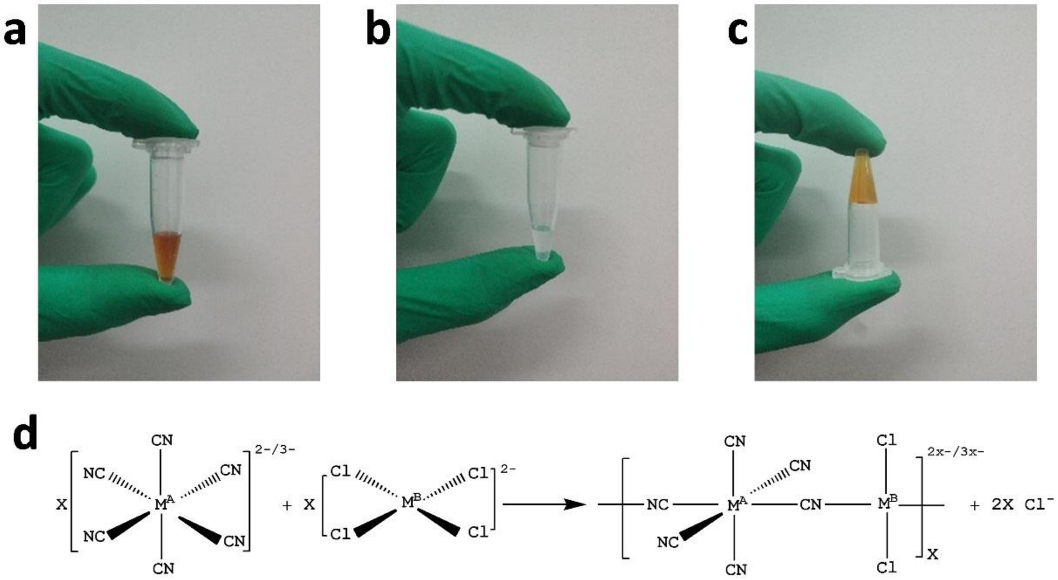

Figure S1. Photographs of **(a)** H_2PdCl_4 solution, **(b)** $K_3Co(CN)_6$ solution and **(c)** PdCo cyanogel. **(d)** The equation of the formation of cyanogel via the reaction between cyanometalate $[M^A(CN)_n]^{2-/3-}$ (n=4 or 6, M^A= Fe, Co, Ni, Pd, Ru, Os and Cr) and chlorometalate $[M^BCl_4]^{2-}$ (M^B = Pd and Pt).

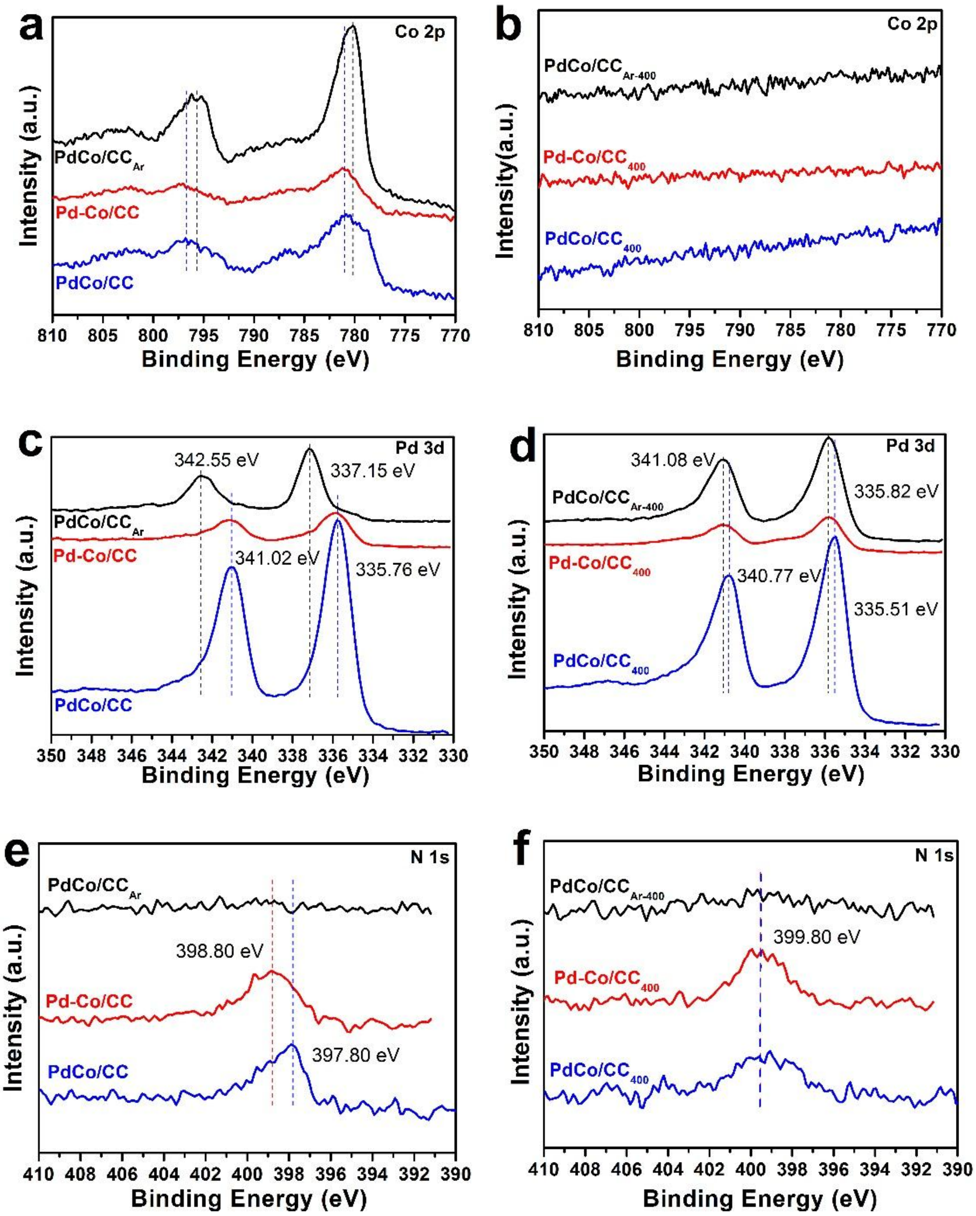

Figure S2. XPS core level spectra for Co 2p **(a, b)**, Pd 3d **(c, d)**, and N 1s **(e, f)** of PdCo$_{Ar}$/CC, Pd-Co/CC, PdCo/CC samples before **(a, c, e)** and after **(b, d, f)** EC scanning treatment for 400 cycles in 0.5 M H_2SO_4.

Compared the Co 2p signals in Figure S2a and S2b, it can be noticed that the Co species in all PdCo$_{Ar}$/CC, Pd-Co/CC, PdCo/CC samples are disappeared after EC scanning treatment in acid.

For Pd 3d signals, the peaks are shifted to the lower binding energies. This can be ascribed to the successful dealloy process by dissolving Co species. Furthermore, it should be noted that the Pd 3d signals from PdCo/CC process a lower binding energy compared to PdCo/CC$_{Ar}$.

For N 1s peaks of Pd-Co/CC and PdCo/CC are shifted to the higher binding energies. This is originated from the dissolution of Co-N (~397.7 eV). And the remained N 1s signals (~ 399.50) are originated from the N-doped CC (i.e. N-(C)$_3$ and C=N-C).

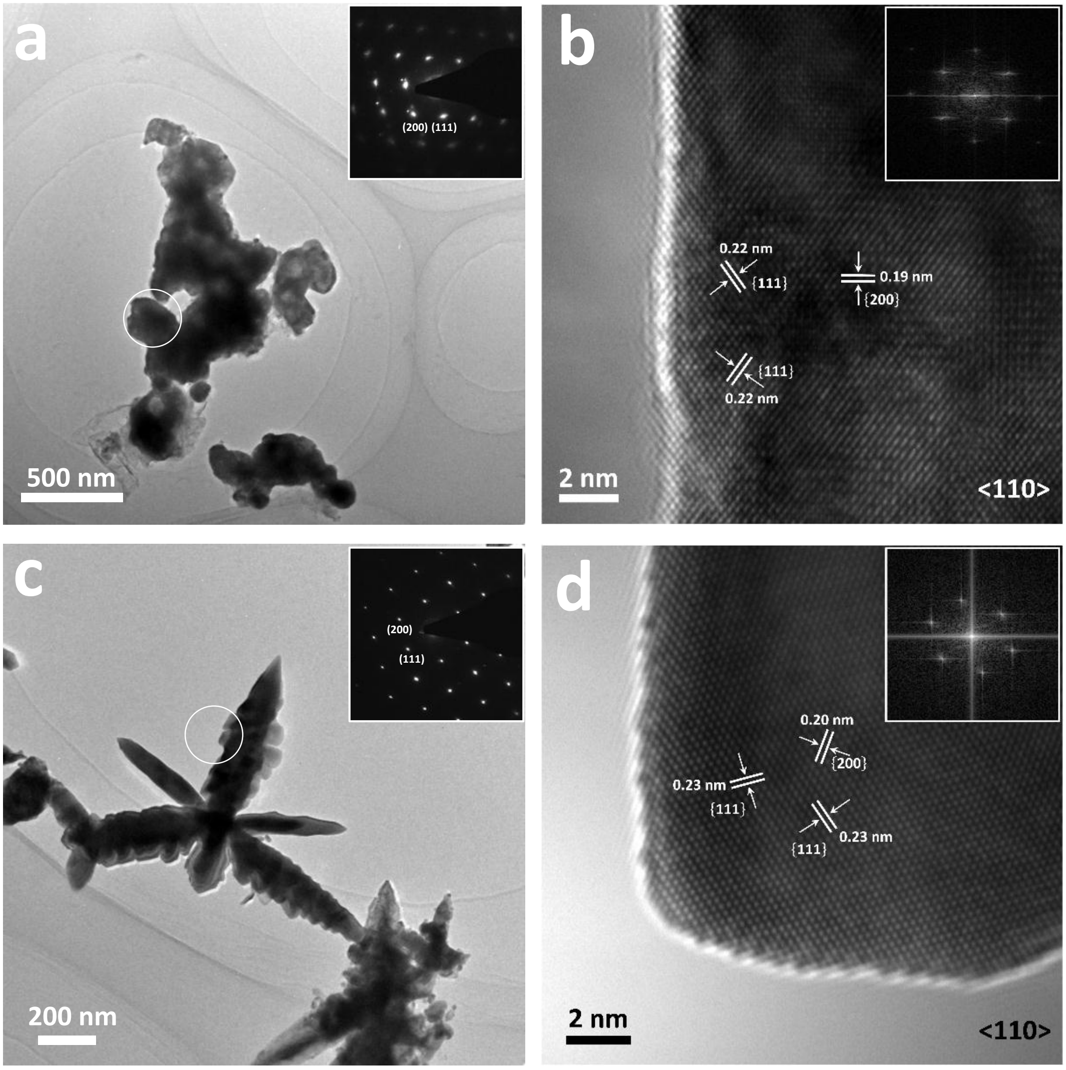

Figure S3. TEM image of **(a)** PdCo/CC and **(c)** PdCo/CC$_{400}$ viewed along along <110> direction. Inset is electron-diffraction pattern recorded on the region indicated with the white circle. High-resolution TEM image of **(b)** PdCo/CC and **(d)** PdCo/CC$_{400}$. Inset is the corresponding FFT pattern.

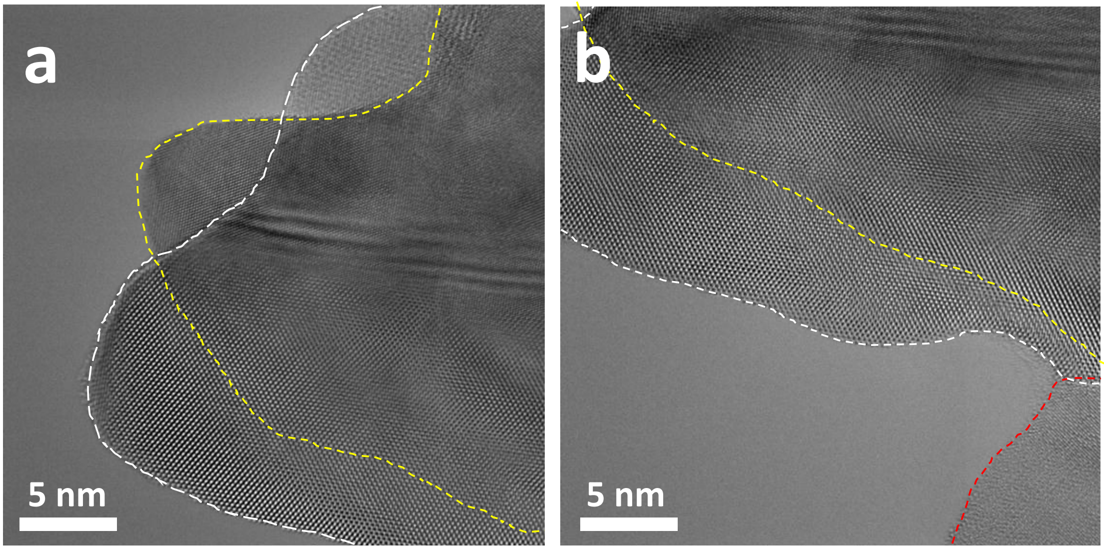

Figure S4. Aberration-corrected HR-TEM image of PdCo/CC_{400} viewed along along <110> direction showing overlayer of several ultrathin nanosheets.

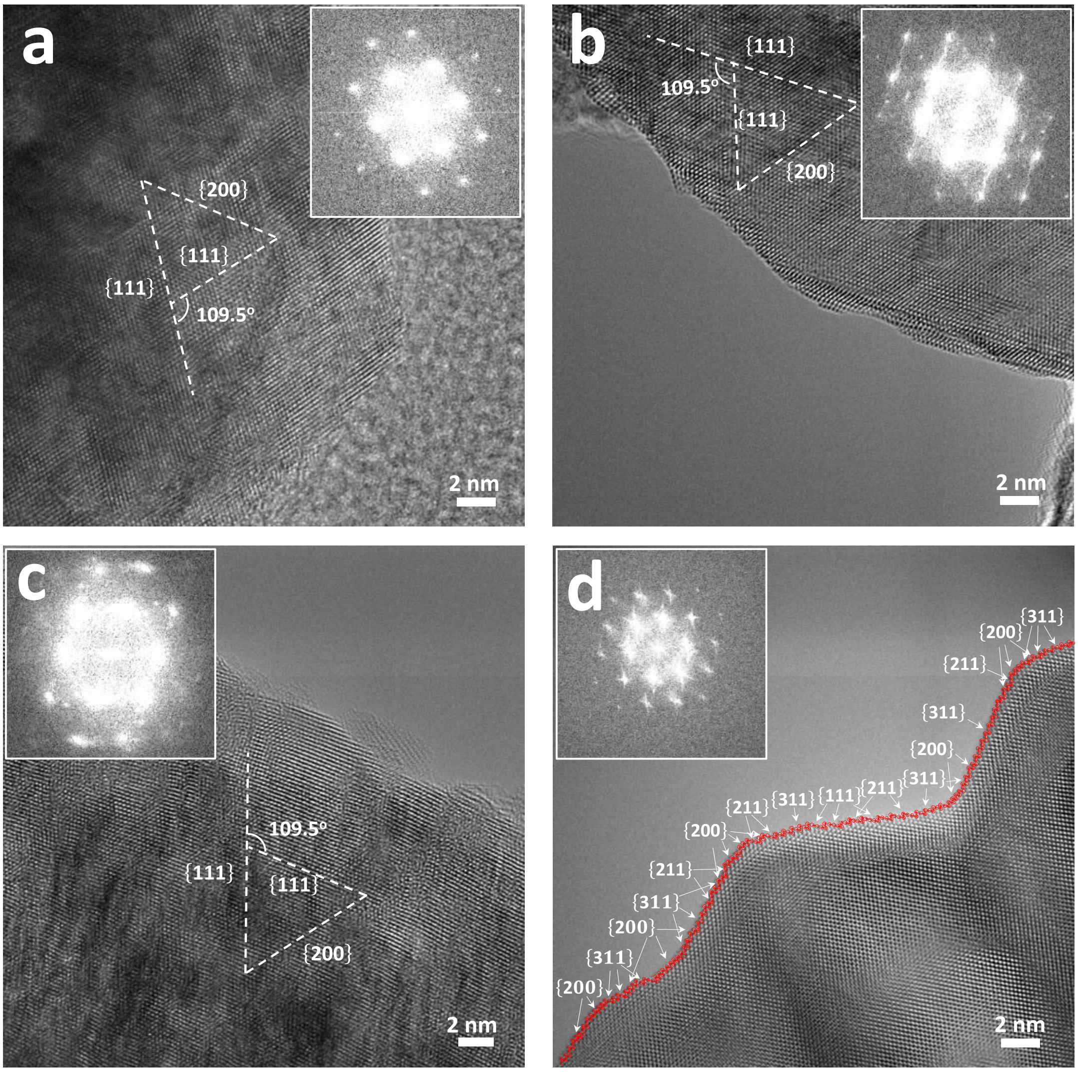

Figure S5. Aberration-corrected HR-TEM image of **(a, b, c)** PdCo/CC and **(d)** PdCo/CC$_{400}$ viewed along along <110> direction showing their surface atomic steps made of different facets. Inset is the corresponding FFT pattern.

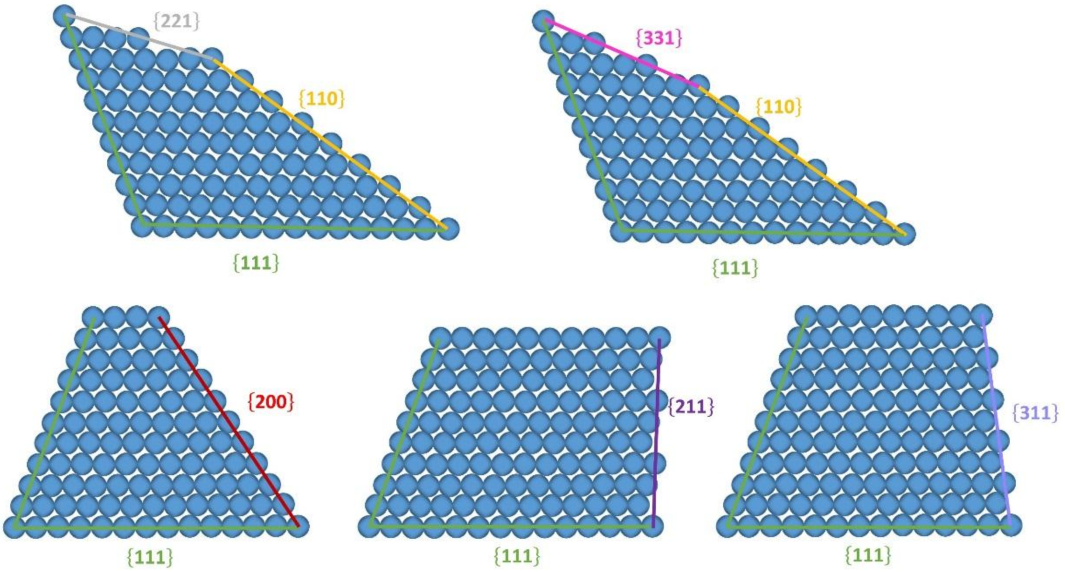

Figure S6. The atomic model of {221}, {331}, {200}, {211} and {311} planes viewed from the <110> directions.

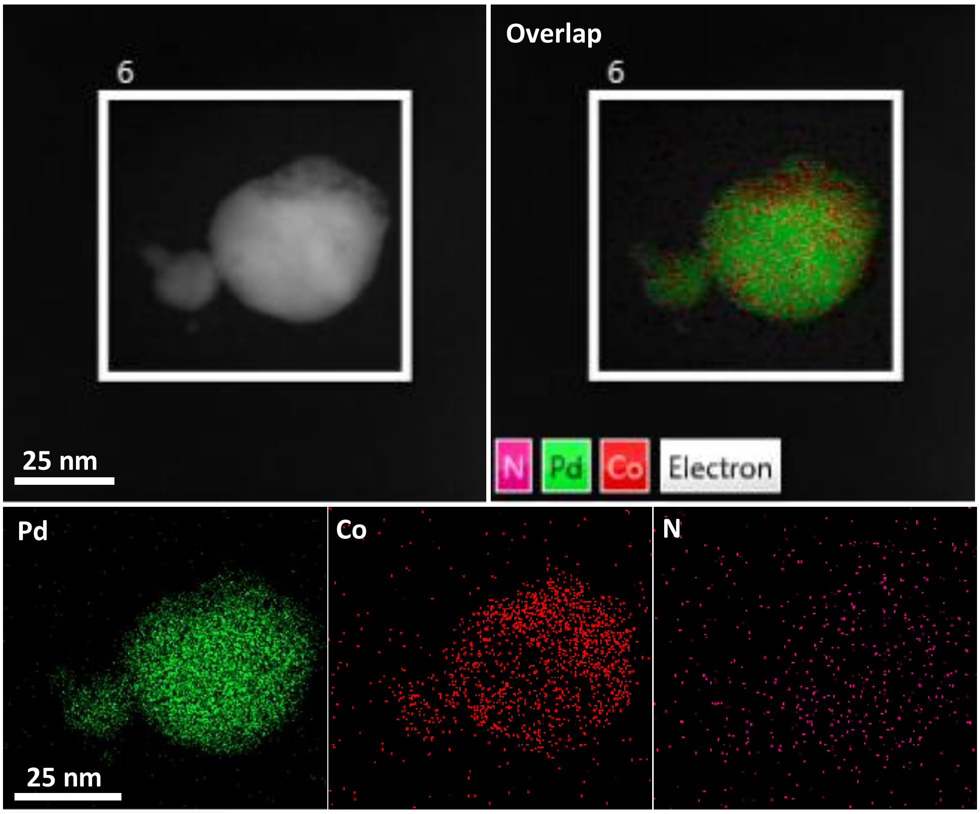

Figure S7. HAADF-STEM elemental mapping of Pd (L), Co (K) and N (K) in PdCo/CC.

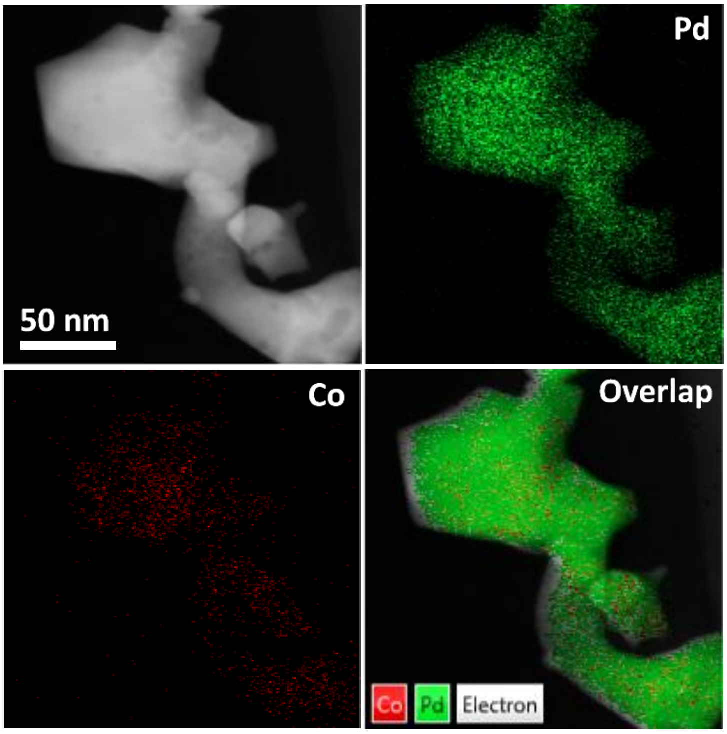

Figure S8. HAADF-STEM elemental mapping of Pd (L), Co (K) in PdCo/CC_{400}.

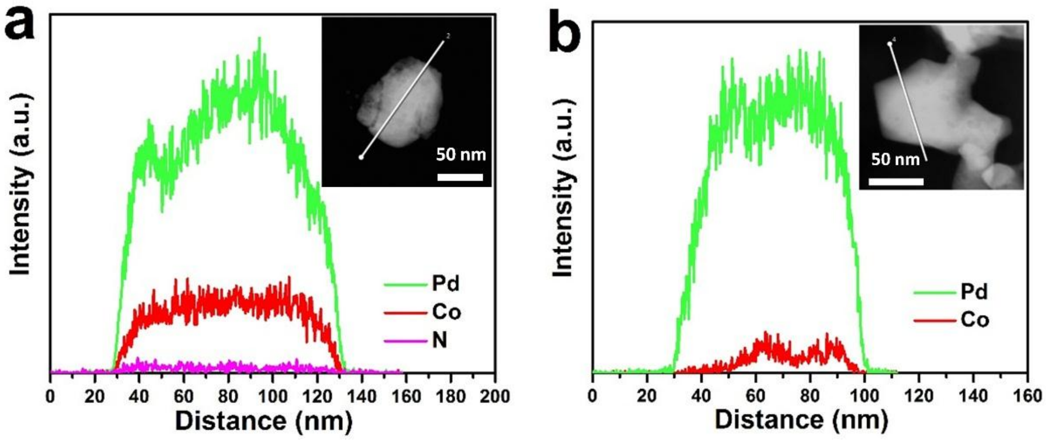

Figure S9. Line scan analysis of **(a)** PdCo/CC and **(b)** PdCo/CC$_{400}$.

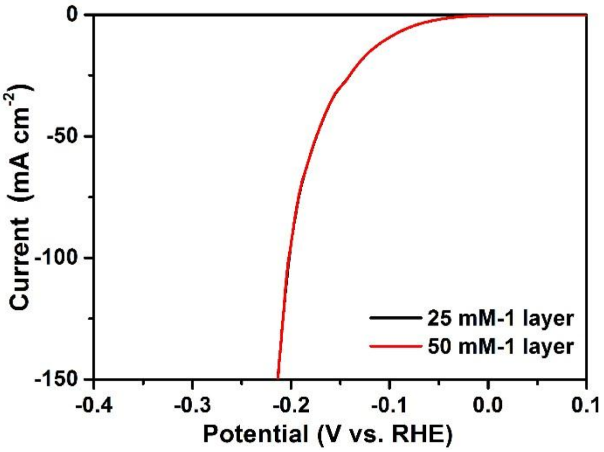

Figure S10. HER polarization curves of PdCo/CC samples which are prepared with different concentrations of cyanogel precursor.

When the H_2PdCl_4 and $K_3Co(CN)_6$ concentration is less than 25 mM, the stable cyanogel cannot be formed. Further inceasing the precursor concentration, no obvious enhancement in HER catalytical activities is obtained. Therefore, 25 mM H_2PdCl_4 and 25 mM $K_3Co(CN)_6$ is used as the optimized concentration in this work.

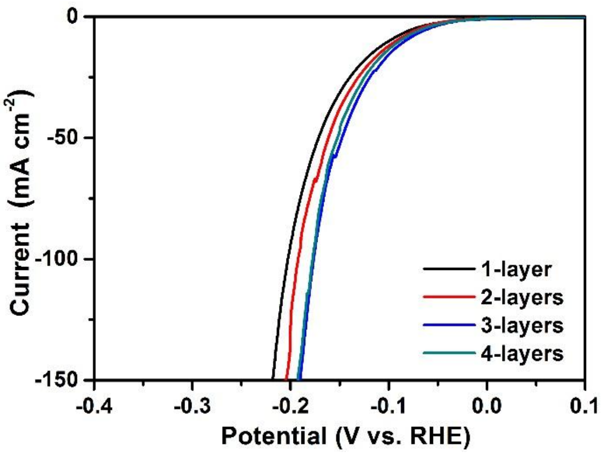

Figure S11. HER polarization curves of PdCo/CC samples which are prepared by different cyanogel coating layers.

It can be noticed that the catalytical activity of the 3-layers sample is similar with the 4-layers sample. Therefore, the cyanogel coating procedure was carried our for three times in this work.

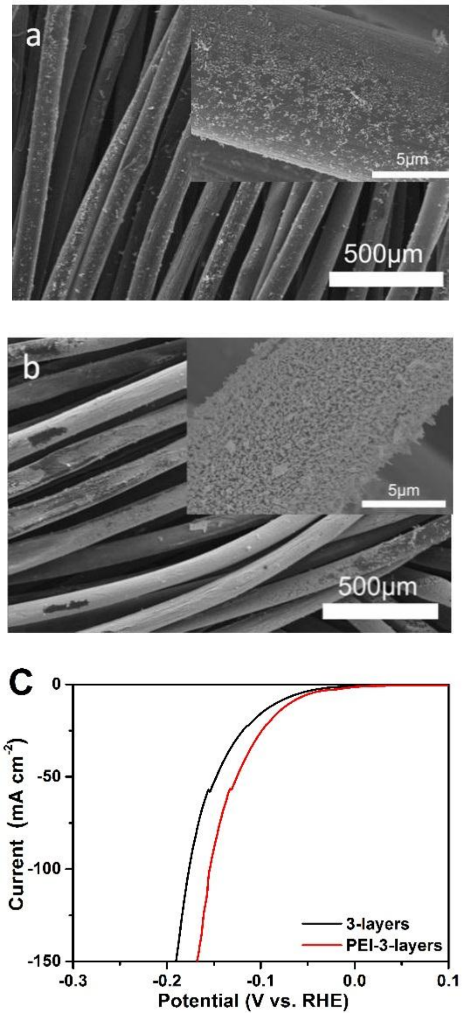

Figure S12. (a, b) SEM and **(c)** HER polarization curves of PdCo/CC samples prepared without **(a)** and with **(b)** PEI treatment.

It can be noticed that the PEI treated CC exhibited a higher HER catalytical activity, which might be attributed to the electrostatic attraction between positively charged PEI with the negatively charged cyanogels, which resulted more uniform cyanogel grafting with a high density.

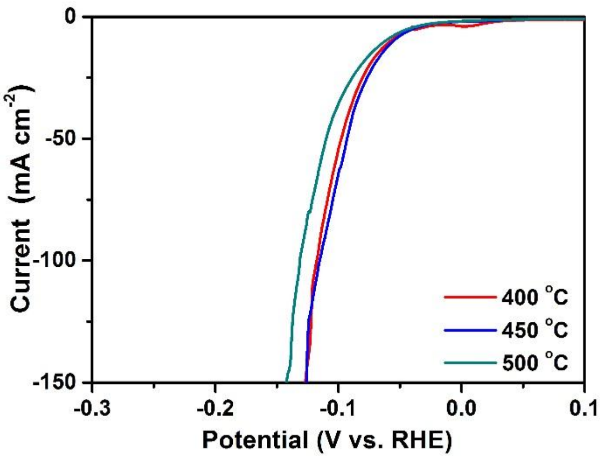

Figure S13. HER polarization curves of PdCo/CC samples prepared at different annealling temperature in NH_3 atmosphere.

From the comparison of overpotantial, it can be noticed that the smallest overpotantial was achieved at the annealling temperature of 450 °C. Therefore, 450 °C was used as the annealing temperature in this work.

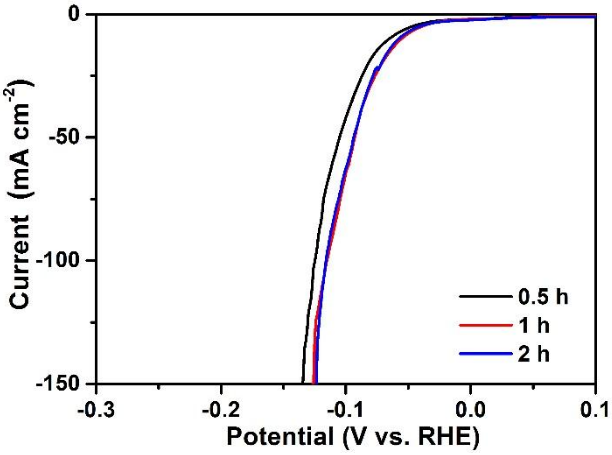

Figure S14. HER polarization curves of PdCo/CC samples prepared by different annealling time in NH_3.

According to the overpotantial values, we chose 1 h for annealling treatment in this work.

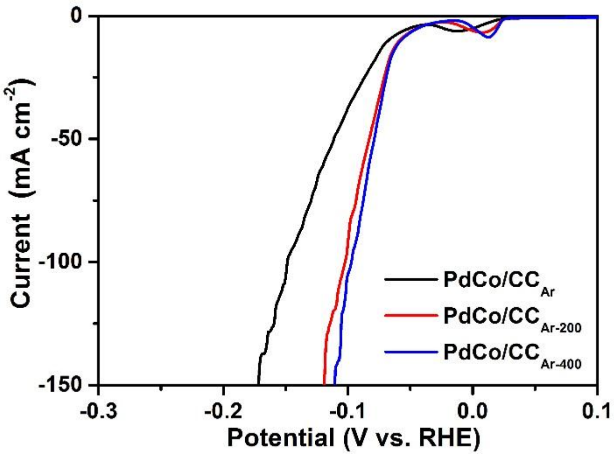

Figure S15. The HER polarization curves of the PdCo/CC$_{Ar}$ samples (annealing under Ar at 450 ^{o}C for 1 h) before and after EC scaning for 200 and 400 cycles.

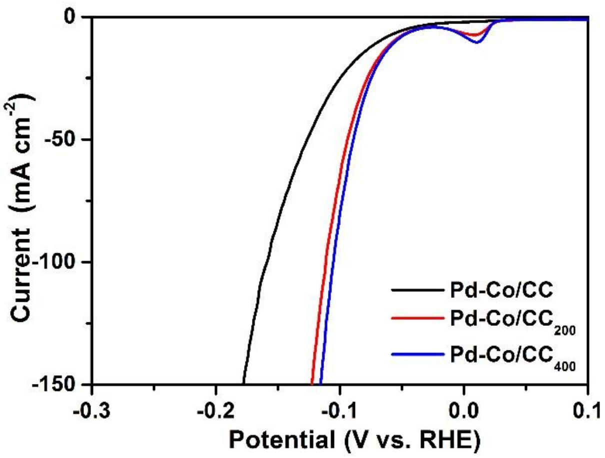

Figure S16. The HER polarization curves of the Pd-Co/CC samples before and after EC scaning for 200 and 400 cycles.

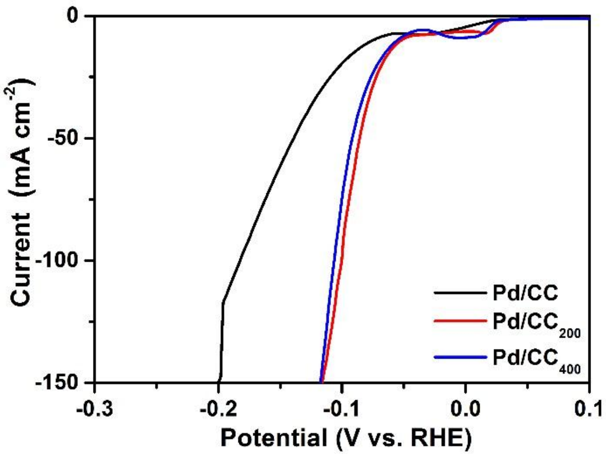

Figure S17. The HER polarization curves of the Pd/CC samples before and after EC scaning for 200 and 400 cycles.

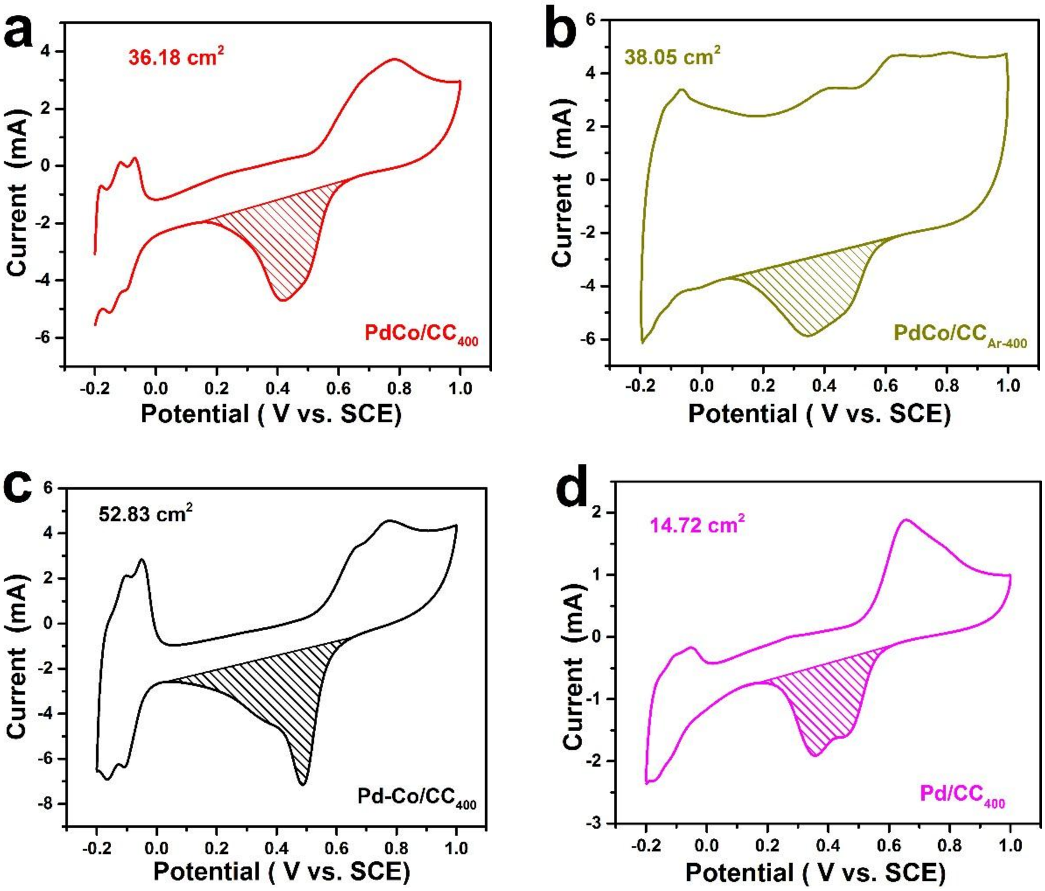

Figure S18. The calculated ECSA of Pd in **(a)** PdCo/CC$_{400}$, **(b)** PdCo/CC$_{Ar400}$, **(c)** Pd-Co/CC$_{400}$ and **(d)** Pd/CC$_{400}$.

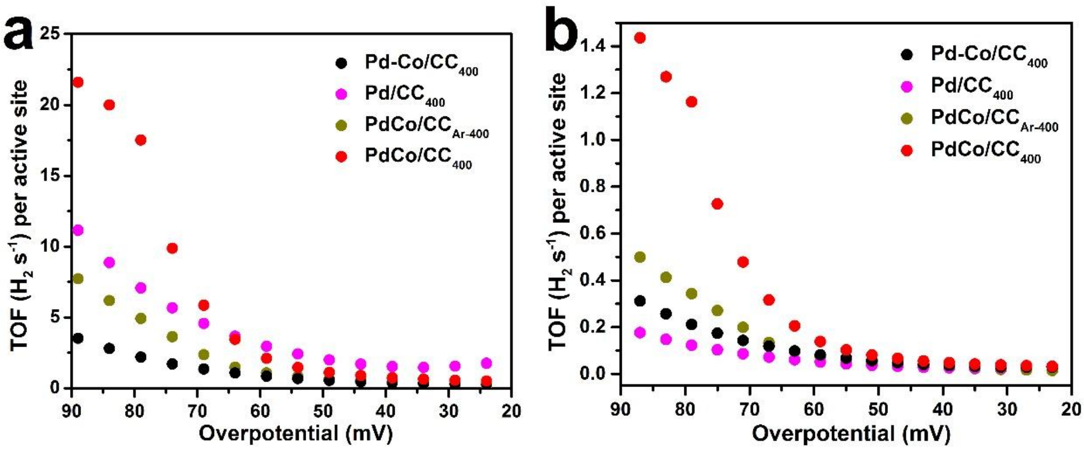

Figure S19. Comparison of the TOF values of PdCo/CC$_{400}$, Pd-Co/CC$_{400}$, Pd/CC$_{400}$, and PdCo/CC$_{Ar400}$. Note that the TOF values were calculated based on the number of active noble-metal atoms using **(a)** ECSA and **(b)** mass loading, respectively.

Table S1. All adsorption configurations and their corresponding adsorption energies (eV) of CN on (100), (110) and (111) surfaces of Pd and fcc-Co.

CN	Most stable structure	Other tested structures	
Pd(100)	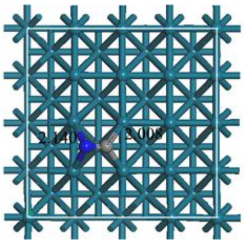 Eads=-4.36 eV	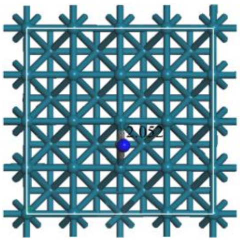 Eads=-3.79 eV	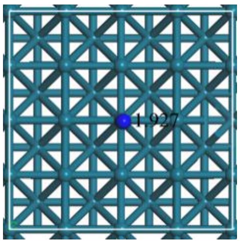 Eads=-3.44 eV
Pd(110)	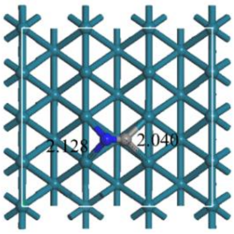 Eads=-4.58 eV	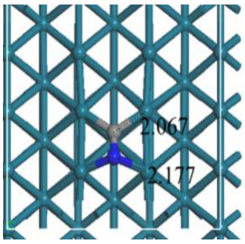 Eads=-4.11 eV 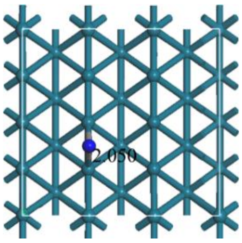 Eads=-3.78 eV	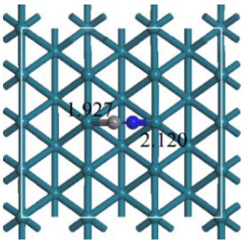 Eads=-4.00 eV 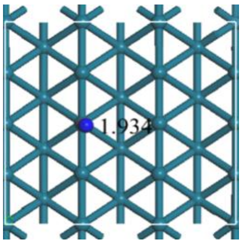 Eads=-3.49 eV
Pd(111)	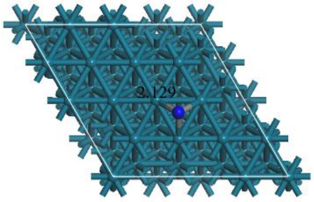 Eads=-3.81 eV	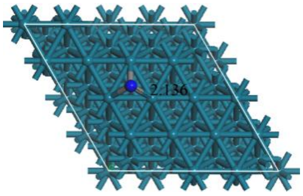 Eads=-3.74 eV	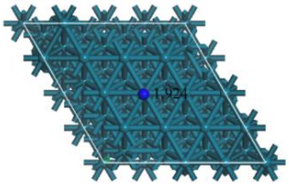 Eads=-3.39 eV
Co(100)	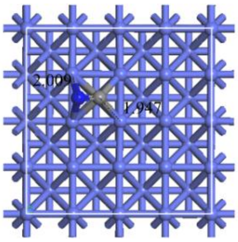 Eads=-4.83 eV	Initially sites (hollow, bridge) not stable	
Co(110)	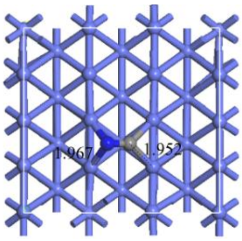 Eads=-4.87 eV	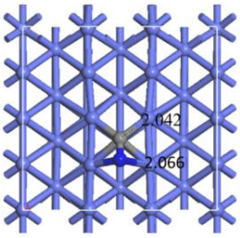 Eads=-4.31 eV	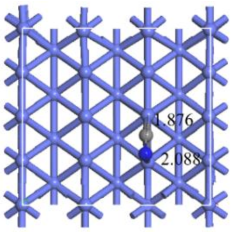 Eads=-4.24 eV

Co(111)	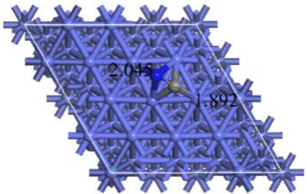 Eads=-4.42 eV	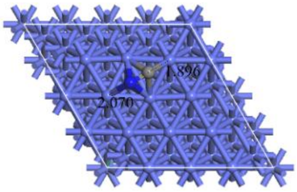 Eads=-4.40 eV 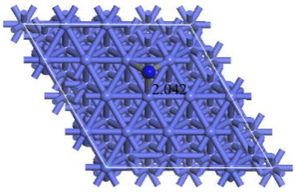 Eads=-4.06 eV

Table S2. All adsorption configurations and their corresponding adsorption energies (eV) of NH_3 on (100), (110) and (111) surfaces of Pd and fcc-Co.

NH_3	Most stable structure	Other tested structures
Pd(100)	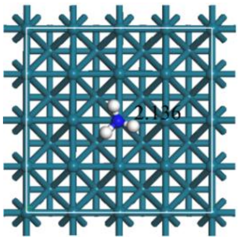 Eads=-0.83 eV	Initially sites (hollow, bridge) not stable
Pd(110)	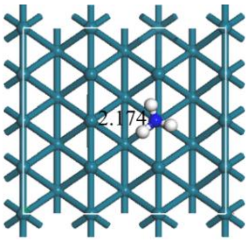 Eads=-0.79 eV	Initially sites (hollow, short-bridge, long-bridge) not stable
Pd(111)	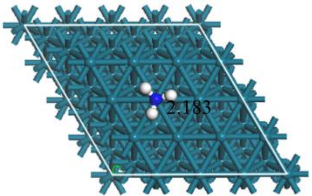 Eads=-0.77 eV	Initially sites (fcc, bridge, hcp) not stable
Co(100)	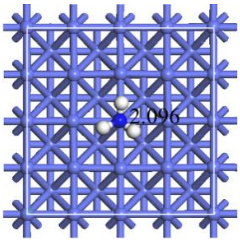 Eads=-0.79 eV	Initially sites (hollow, bridge) not stable
Co(110)	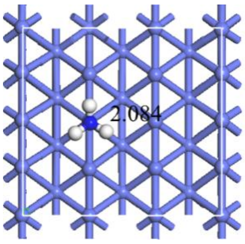	Initially sites (hollow, short-bridge, long-bridge) not stable

	Eads=-0.83 eV	
Co(111)	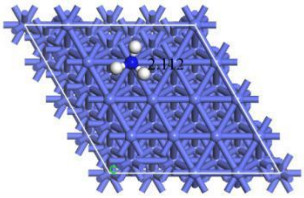 Eads=-0.76eV	Initially sites (fcc, bridge, hcp) not stable.

Table S3. All adsorption configurations and their corresponding adsorption energies (eV) of Ar on (100), (110) and (111) surfaces of Pd and fcc-Co.

Ar	Most stable structure	Other tested structures
Pd(100)	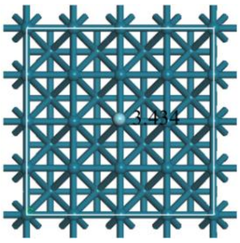 Eads=-0.01 eV	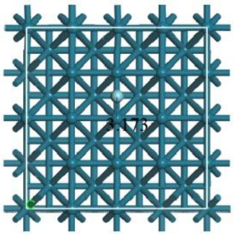 Eads=0 eV 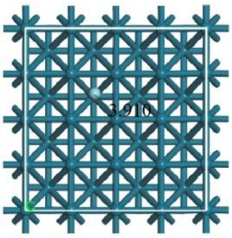 Eads=0 eV
Pd(110)	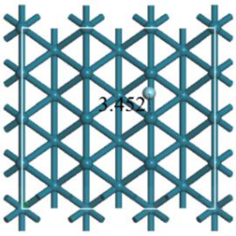 Eads=-0.01 eV	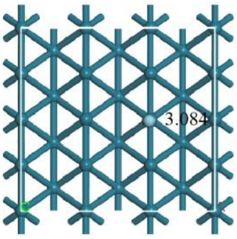 Eads=0 eV 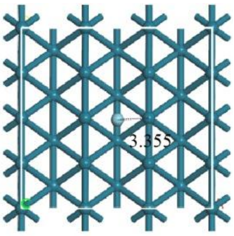 Eads=0 eV 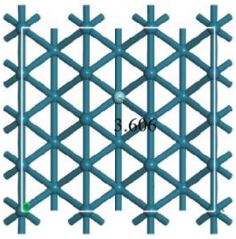 Eads=0 eV
Pd(111)	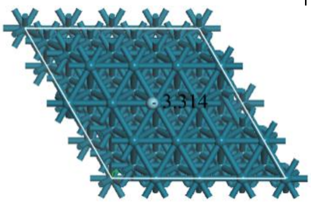 Eads=-0.01 eV	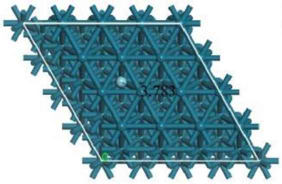 Eads=0 eV 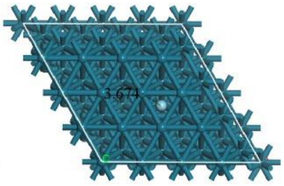 Eads=0 eV 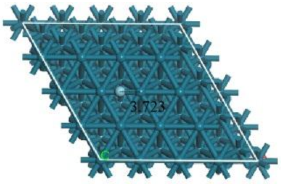 Eads=0 eV

Co(100)	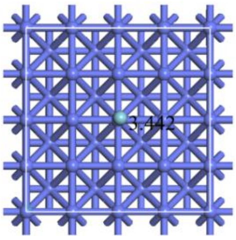 Eads=0 eV	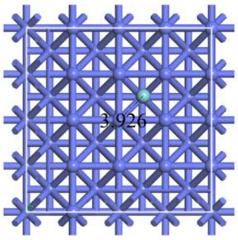 Eads=0 eV 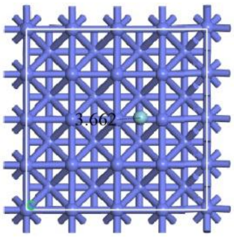 Eads=0 eV
Co(110)	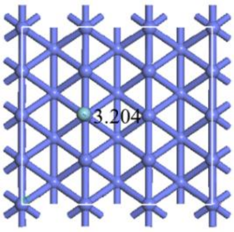 Eads=-0.01 eV	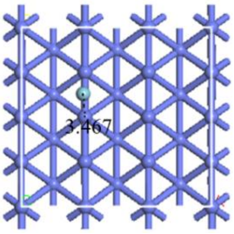 Eads=0 eV 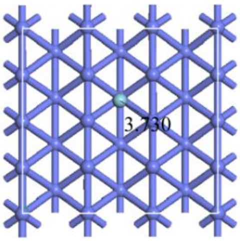 Eads=0 eV 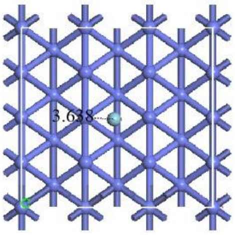 Eads=0 eV
Co(111)	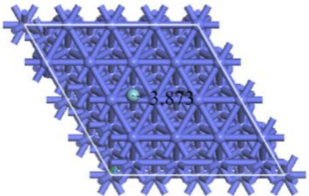 Eads=0 eV	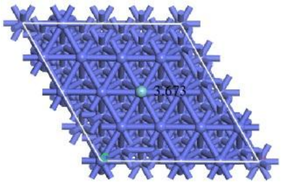 Eads=0 eV 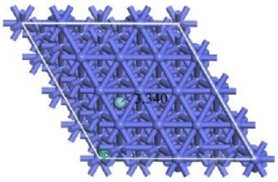 Eads=0 eV 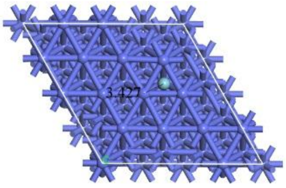 Eads=0 eV

Table S4. SEM images of PdCo/CC$_{Ar}$, Pd-Co/CC, PdCo/CC and Pd/CC samples undergo different EC scanning cycles in 0.5 M H_2SO_4.

	PdCo/CC$_{Ar}$	Pd-Co/CC	PdCo/CC	Pd/CC
0 CVs	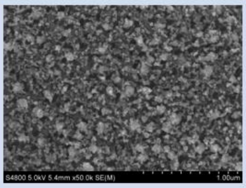	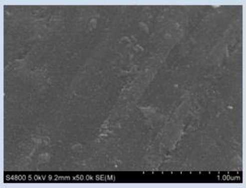	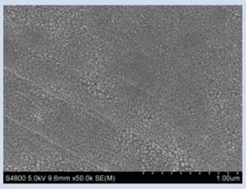	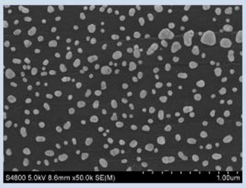
200 CVs	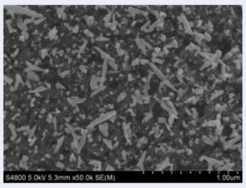	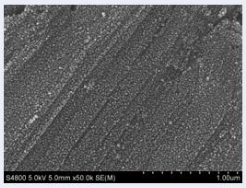	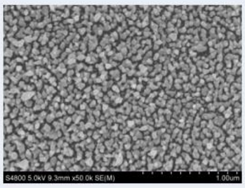	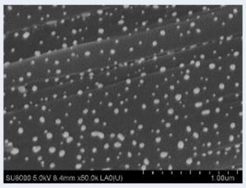
400 CVs	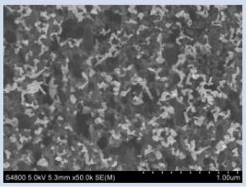	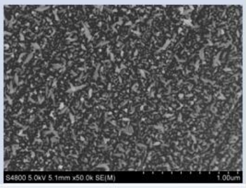	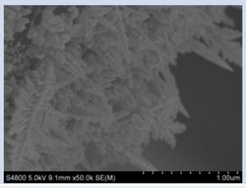	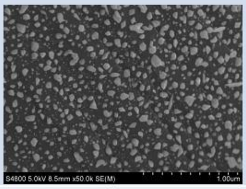
1000 CVs	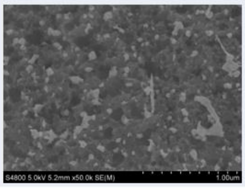	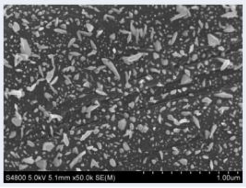	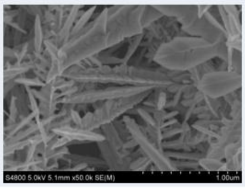	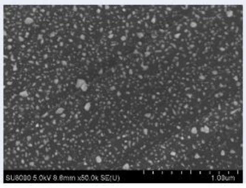

Table S5. The supercells of the (211) (221) (311) (331) crystal faces of Pd, the corresponding surface area, and the number of step sites per supercell.

	facet	supercell/Å	surface area/Å^2	Number of step sites
Pd	211	a=13.48,b=11.01	148.32	5
	221	a=11.01,b=16.51	181.65	5
	311	a=9.53,b=11.01	100.41	4
	331	a=11.01,b=12.30	131.97	4

Comparison of number (*N*) of step site per area

N_{211}/N_{221} = (5/148.32)/(5/181.65) = 181.65/148.32 = 1.22

N_{311}/N_{331} = (4/100.41)/(4/131.97) = 131.97/100.41 = 1.31

Table S6. Comparison of representative carbon-based HER and other noble metal catalysts in 0.5 M H_2SO_4.

	Loading (mg cm^{-2})	Tafel slope (mV dec^{-1})	Current Density (mA cm^{-2})	Overpotential (mV)	Ref
porous Pd-CNx	0.043	35	50	85	S4
Pd cube/PEI-rGO 50:1 (10 wt. %)	0.141	34	100	98	S5
Au@PdAg NRBs	0.035	30	60	60	S6
Ni@Pd4:1/PEI–rGO 50:1 (10 wt. %)	0.141	54	100	130	S7
Pt–Pd–rGO	/	10	100	77	S8
RhCo-ANAs	2	30.7	100	62	S9
Pt-NPs	2	30.3	100	79	S9
IrP_2@NC	0.7	28	50	35	S10
Ru/ NG-750	/	44	40	95	S11
Ru@C_2N	0.285	30	30	46	S12
29.1 wt% Rh/SiNW	0.193	24	100	177	S13
40 wt% Pt/C	0.193	30	100	179	S13
Pt sheet	/	37.2	100	90	This work
Pt/C$_{(20\%)}$	0.125	31.7	100	75	This work
PdCo/CC$_{400}$	0.125	22.8	100	75	This work

Table S7. Comparison of TOF for the HER on different catalyst before and after 400 EC scanning cycles in 0.5 M H_2SO_4.

	TOF@η=70 mV (s^{-1})	TOF@η=75 mV (s^{-1})
Pd-Co/CC$_{400}$	1.40	1.80
Pd/CC$_{400}$	4.76	5.92
PdCo/CC$_{Ar\text{-}400}$	2.62	3.87
PdCo/CC$_{400}$	6.48	10.96

References

[1] Y. Xu, M. Gao, Y. Zheng, J. Jiang, S. Yu, *Angew. Chem. Int. Ed.*, 2013, **52**, 8546-8550.

[2] H. Liao, C. Wei, J. Wang, A. Fisher, T. Sritharan, Z. Feng, Z. J. Xu, *Adv. Energy Mater.*, 2017, **7**, 1701129.

[3] J. Fan, K. Qi, L. Zhang, H. Zhang, S. Yu, X. Cui, *ACS Appl. Mater. Interfaces*, 2017, **9**, 18008-18014.

[4] T. Bhowmik, M. K. Kundu, S. Barman, *ACS Catal.*, 2016, **6**, 1929-1941.

[5] J. Li, P. Zhou, F. Li, J. Ma, Y. Liu, X. Zhang, H. Huo, J. Jin, J. Ma, *J. Power Sources*, 2016, **302**, 343-351.

[6] Z. Fan, Z. Luo, X. Huang, B. Li, Y. Chen, J. Wang, Y. Hu, H. Zhang, *J. Am. Chem. Soc.*, 2016, **138**, 1414-1419;

[7] J. Li, P. Zhou, F. Li, R. Ren, Y. Liu, J. Niu, J. Ma, X. Zhang, M. Tian, J. Jin, J. Ma, *J. Mater. Chem. A*, 2015, **3**, 11261-11268.

[8] S. Bai, C. Wang, M. Deng, M. Gong, Y. Bai, J. Jiang, Y. Xiong, *Angew. Chem., Int. Ed.*, 2014, **53**, 12120-12124.

[9] Y. Zhao, J. Bai, X.-R. Wu, P. Chen, P.-J. Jin, H.-C. Yao and Y. Chen, *J. Mater. Chem. A*, 2019, **7**, 16437-16446.

[10] Z. Pu, J. Zhao, I. S. Amiinu, W. Li, M. Wang, D. He and S. Mu, *Energy Environ. Sci.*, 2019, **12**, 952-957.

[11] R. Ye, Y. Liu, Z. Peng, T. Wang, A. S. Jalilov, B. I. Yakobson, S.-H. Wei and J. M. Tour, *ACS Appl. Mater. Interfaces*, 2017, **9**, 3785-3791.

[12] J. Mahmood, F. Li, S.-M. Jung, M. S. Okyay, I. Ahmad, S.-J. Kim, N. Park, H. Y. Jeong and J.-B. Baek, *Nat. Nanotechnol.*, 2017, **12**, 441.

[13] L. Zhu, H. Lin, Y. Li, F. Liao, Y. Lifshitz, M. Sheng, S.-T. Lee and M. Shao, *Nat. Commun.*, 2016, **7**, 12272.